Deep-Sea Research I 57 (2010) 869–879

Contents lists available at ScienceDirect

Deep-Sea Research I

journal homepage: www.elsevier.com/locate/dsri

Arctic ocean shelf–basin interaction: An active continental shelf CO_2 pump and its impact on the degree of calcium carbonate solubility

L.G. Anderson [a,*], T. Tanhua [b], G. Björk [c], S. Hjalmarsson [a], E.P. Jones [d], S. Jutterström [a], B. Rudels [e], J.H. Swift [f], I. Wåhlström [a]

[a] Department of Chemistry, University of Gothenburg, Sweden
[b] Leibniz Institute of Marine Sciences, Kiel, Germany
[c] Earth Sciences Center, University of Gothenburg, Sweden
[d] Bedford Institute of Oceanography, Halifax, Canada
[e] Finnish Meteorological Institute, Helsinki, Finland
[f] Scripps Institution of Oceanography, University of California San Diego, La Jolla, CA, USA

ARTICLE INFO

Article history:
Received 30 November 2009
Received in revised form
25 March 2010
Accepted 29 March 2010
Available online 8 April 2010

Keywords:
Arctic Ocean
Marine carbon system
Continental shelf pump

ABSTRACT

The Arctic Ocean has wide shelf areas with extensive biological activity including a high primary productivity and an active microbial loop within the surface sediment. This in combination with brine production during sea ice formation result in the decay products exiting from the shelf into the deep basin typically at a depth of about 150 m and over a wide salinity range centered around $S \sim 33$. We present data from the Beringia cruise in 2005 along a section in the Canada Basin from the continental margin north of Alaska towards the north and from the International Siberian Shelf Study in 2008 (ISSS-08) to illustrate the impact of these processes. The water rich in decay products, nutrients and dissolved inorganic carbon (DIC), exits the shelf not only from the Chukchi Sea, as has been shown earlier, but also from the East Siberian Sea. The excess of DIC found in the Canada Basin in a depth range of about 50–250 m amounts to 90 ± 40 g C m^{-2}. If this excess is integrated over the whole Canadian Basin the excess equals $320 \pm 140 \times 10^{12}$ g C. The high DIC concentration layer also has low pH and consequently a low degree of calcium carbonate saturation, with minimum aragonite values of 60% saturation and calcite values just below saturation. The mean age of the waters in the top 300 m was calculated using the transit time distribution method. By applying a future exponential increase of atmospheric CO_2 the invasion of anthropogenic carbon into these waters will result in an under-saturated surface water with respect to aragonite by the year 2050, even without any freshening caused by melting sea ice or increased river discharge.

1. Introduction

The world oceans together with the atmosphere are the main sink of anthropogenic carbon. The oceanic uptake of anthropogenic carbon dioxide equals the difference between the air–sea flux of CO_2 today and that of pre-industrial times (e.g. Anderson and Olsen, 2002). All oceanic regions have to be considered when estimating this uptake, including the very dynamic continental shelf seas. The sequestration of carbon by the deep oceans can occur by two processes, either by transport of water (both vertically by deep convection and along isopycnal surfaces) with its content of excess dissolved carbon species, or by vertical flux of particulate matter containing carbon. The latter flux is dominated by sinking organic matter formed by biological production, which in the oceans is largely limited by nutrients (micro or macro). Any change in the vertical C-particle flux, for example changes in climate or nutrient supply, will thus impact the oceanic uptake of anthropogenic CO_2.

Coastal seas around the globe are among the most biologically productive areas as a result of nutrient supply from surrounding land and upwelling of nutrient rich waters from the continental slope (Walsh, 1991; Mackenzie et al., 1998; De Haas et al., 2002; Chen and Borges, 2009). However, the dynamic conditions that prevail in the shelf regions make it difficult to translate this high productivity into a general statement about its role as sink of atmospheric CO_2. In extreme situations a shelf area might be transformed from a source to a sink of CO_2 (or vice versa) within a week and over distances of kilometers (Kempe, 1995; Kempe and Pegler, 1991). The potential sink or source status of a continental shelf is determined by several complex factors, such as input of

* Corresponding author.
E-mail address: leifand@chem.gu.se (L.G. Anderson).

0967-0637/$ - see front matter © 2010 Elsevier Ltd. All rights reserved.
doi:10.1016/j.dsr.2010.03.012

terrestrial organic matter (OM), marine OM production, mineralization of OM, and transport and exchange of OM and dissolved organic and inorganic carbon. Generally, the near shore coastal and estuarine environments tend to be sources of CO_2 to the atmosphere while offshore coastal shelf regions tend to be sinks (Borges and Frankignoulle, 1999, 2002; Ducklow and McAllister, 2005; Borges et al., 2005; Semiletov et al., 2007; Chen and Borges, 2009).

It is difficult to compute the air–sea flux in such a variable region from measured partial pressure difference of CO_2 (ΔpCO_2) between the atmosphere and the surface water with any accuracy without a very demanding measurement program having high resolution in both space and time. The fate of the organic matter produced over or added to the shallow continental shelves are remineralization and vertical mixing of the decay products and dissolved organic carbon (DOC) back to the surface mixed layer, burial in the sediment and remineralization with the decay products and DOC staying in the higher density shelf bottom water. The latter water is subsequently exported along isopycnal surfaces or follows the bottom into the neighboring deep basin. Consequently, the net result of uptake of CO_2 from the atmosphere is that the carbon ends up either in the sediment or as an increased storage in the water column that eventually will be exported into the neighboring deep ocean. The importance of the last process, the continental shelf pump, has been a topic for discussion (Tsunogai et al., 1999; Wang et al., 2000; Frankignoulle and Borges, 2001; Bozec et al., 2005) and has been quantified based on air–sea flux computations, for example for the North Sea (Thomas et al., 2004).

The Arctic shelves experience special conditions compared to the rest of the global coastal seas. First they are extremely wide, second they are mostly covered by sea ice except during the summer season, and last much terrestrial organic matter is added by river runoff and coastal erosion. However, they have in common with other shelf seas that some parts are very productive. This is the situation in especially the Chukchi and Barents Seas that are defined as inflow shelves (Carmack and Wassmann, 2006), and thus gets a continuous supply of nutrients by the inflow from the Pacific and Atlantic Oceans, respectively. In these seas the retreating sea ice in spring creates very favorable conditions for primary production, called the Marginal Ice Zone bloom (Wassmann et al., 2006; Wang et al., 2005). Primary production consumes CO_2 and thereby lowers the partial pressure of CO_2 (pCO_2), often leading to an under saturation relative to the atmospheric pCO_2. As the surface water continues into the central Arctic Ocean, which is largely ice covered also in the summer, the exchange with the atmosphere is hampered and the surface water remains under-saturated (Kaltin and Anderson, 2005; Bates, 2006).

The Arctic Ocean and especially its vast shelves are subjected to changes in the physical setting (temperature, salinity, sea ice coverage) as a result of shifts in the climate conditions. The Chukchi Sea and its northern continental slope have experienced large decrease in the summer sea ice coverage during the recent years (http://nsidc.org/arcticseaicenews/) that has been shown to have a major impact on the primary productivity of the region (Wang et al., 2005). These changes have a potential to significantly alter the fluxes of carbon not only by increasing primary production but also by air–sea CO_2 flux (e.g. Anderson and Kaltin, 2001; Hill and Cota. 2005; Bates, 2006; Mathis et al., 2007b).

The Pacific Sector of the Arctic Ocean (Fig. 1) is a region where the export of carbon and nutrients from the continental shelf pump is easily detected. A persistent nutrient maximum has been observed in depth profiles within the Canadian Basin of the Arctic Ocean centered around a salinity of 33.1 (e.g. Nikiforev et al., 1966; Meĺnikov and Pavlov, 1978; Kinney et al., 1970; Moore et al., 1983; Jones and Anderson, 1986; Codispoti et al., 2005; Mathis et al., 2007a; Lepore et al., 2007). This nutrient maximum has been suggested to be a result of a combination of extensive primary production in the Chukchi Sea region followed by decay of organic matter at the sediment surface (e.g. Jones and Anderson, 1986). Brine production from sea ice formation can produce a saline bottom water which has an overlying water of low salinity that hampers vertical mixing of the decay products back into the photic zone within the shelf seas. This relatively high salinity bottom water with elevated nutrient content flows towards and out into the deep Arctic Ocean.

Within the deep Arctic Ocean this nutrient rich layer, known as the upper halocline layer (UHL), underlies the polar mixed layer (PML) that is a mixture of waters from the surrounding oceans (mainly the Pacific Ocean within this study area), river runoff and sea ice meltwater. Below the UHL are the lower halocline layer (LHL) and the Atlantic water layer (AWL), which are both of Atlantic origin (e.g. Rudels et al., 2004; Carmack and Wassmann, 2006). The general circulation patterns of UHL, LHL and AWL have been suggested to follow the continental margin and underwater ridges in a counterclockwise circulation around the Arctic Ocean (Rudels et al., 1994, 1996). This flow pattern has likely much small scale variability that is highly patchy in time and there is not even one single source of any of these waters. In the Canadian Basin is the PML, on the other hand, more or less trapped within the Beaufort Gyre (Jones et al., 1998), but with an extent that is highly dependent on wind forcing (Proshutinsky and Johnson, 1997; Proshutinsky et al., 2002).

The sources and circulation of the different waters determine the chemical composition, for which the PML of the study area thus is North Pacific Water, mixed with river runoff and sea ice meltwater. The PML probably flows off the Chukchi and East Siberian Seas region into the deep Arctic Ocean in variable paths, largely depending on wind conditions. The water supplying the UHL on the other hand is likely to be more confined to specific regions depending on the bottom topography. Such areas are the Herald Valley, Central Channel and Barrow Canyon, where the latter has been extensively studied within the western Arctic shelf–basin interaction (SBI) project (e.g. Grebmeier and Harvey, 2005). Once the water leaves the shelf and is incorporated in the continental margin current it can be mixed into the central Canadian Basin by eddies formed from this boundary current (Mathis et al., 2007a).

In this contribution we use hydrographic and tracer observations to identify the outflow and fate of carbon from the continental shelf in the Chukchi and East Siberian Seas region of the Arctic Ocean and then use this information to quantify the flux as well as to assess the potential impact by climate change.

2. Methods

The data were collected during the Beringia transpolar cruise on board the Swedish icebreaker Oden from 21 August to 20 September 2005 with complementary data from the western Chukchi Sea and eastern East Siberian Sea region collected during the International Siberian Shelf Study in 2008 (ISSS-08) from the Russian vessel Yacob Smirnitskyi in September 2008. Hydrographic casts were for both cruises performed using a Sea-bird 9/11 CTD to which a 36-bottle rosette sampler was mounted during the Oden cruise and a 12-bottle rosette sampler during the ISSS-08cruise. Water sample analysis for both cruises included dissolved oxygen, nutrients, total dissolved inorganic carbon (DIC), total alkalinity (TA), pH and transient tracers (CFC-11, CFC-12, CFC-113, CCl_4 and SF_6). The transient tracer data from the ISSS-08 cruise are not presented here.

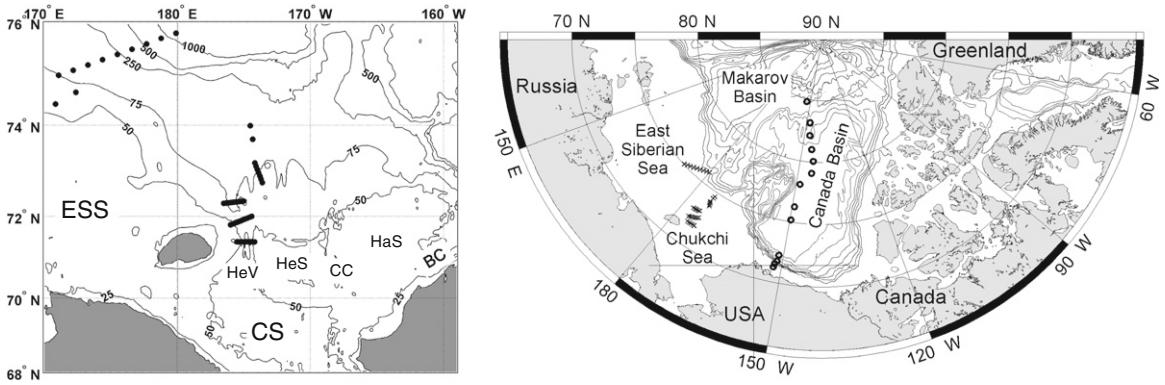

Fig. 1. Map of the study area in the Arctic Ocean. To the right a view of the western Arctic Ocean with station locations discussed in this contribution noted, o are the Beringia 2005 cruise and x are the ISSS-08 cruise. To the left is a blow up of the eastern East Siberian Sea (ESS) and the Chukchi Sea (CS) with the stations visited during ISSS-08 noted. The individual regions noted are Herald Valley (HeV), Herald Shoal (HeS), Central Channel (CC), Hanna Shoal (HaS) and Barrow Canyon (BC).

The nutrients (phosphate, nitrate, nitrite and silicate) during the Beringia 2005 cruise were determined using an auto-analyzer according to the WOCE protocol (Gordon et al., 1993), with a precision ~1%. During the ISSS-08 cruise nutrients were determined using an automatic spectrophotometric system (SmartChem from Westco). The samples were filtered before being analysed and evaluated by a 6 to 8-point calibration curve, precision being ~1%. Oxygen was determined during both cruises using automatic Winkler titration system, precision ~1 μmol kg^{-1}. DIC was determined by a coulometric titration method based on Johnson et al. (1987), having a precision of ~2 μmol kg^{-1}, with the accuracy set by calibration against certified reference materials (CRM), supplied by A. Dickson, Scripps Institution of Oceanography (USA). TA was determined by potentiometric titration, precision ~2 μmol kg^{-1} (Haraldsson et al., 1997), with the accuracy set the same way as for DIC. pH was determined by spectrophotometric detection of pH (Clayton and Byrne, 1993; Lee and Millero, 1995), having a precision of ~0.003 pH units and the accuracy is set by the equilibrium constants of the indicator. The values presented are on the seawater scale and are normalized to a temperature of 15 °C and atmospheric pressure.

The fugacity of carbon dioxide (fCO_2) was computed from DIC and pH using the software CO2SYS (Lewis and Wallace, 1998) and the constants of Merbach et al. (1973) refit by Dickson and Millero (1987) and is presented at insitu temperature and pressure. The non-ideal correction in computing the fCO_2 values are only considering the CO_2–CO_2 molecule interaction (Weiss, 1974). The software CO2SYS handle different pH scales and constants and are converted to a consistent scale in the computations. The choice of DIC and pH used to calculate fCO_2 is the pair that together with TA and pH gives the best accuracy (Anderson et al., 1999), with a theoretical estimated accuracy of the computed fCO_2 is around 5 μatm. However, as many data have high fCO_2 values and all data are for cold waters the error could be significantly higher, but as we only use the fCO_2 data to show the strong signal the error is not critical.

The saturation level of aragonite and calcite were computed from DIC and pH using the same software, CO2SYS, and constants and are presented at insitu temperature and pressure (Mucci, 1983). The calcium ion concentration is assumed to be proportional to salinity, which underestimate the saturation level somewhat in low salinity surface waters of the Arctic Ocean as river runoff include calcium ions. The exact concentration of calcium ions is not known, but as the total alkalinity concentration of the river runoff is up to 1000 μmol kg^{-1} it could be as high as 500 μmol kg^{-1}.

The data from Beringia cruise is archived at the Clivar and Carbon Hydrographic Data Office (http://whpo.ucsd.edu/index.html) and the data from the ISSS-08 cruise are archived at the PANGEA information system under the EU project EPOCA.

To avoid contamination from surrounding air, samples for CFC were the first to be collected from the Niskin bottles, immediately followed by samples for SF_6. The CFC samples were drawn in 100 mL ground glass syringes, and samples for SF_6 were collected in 1000 mL glass bottles with air-tight lids. The samples were stored in water bath at sub-zero temperatures until analysis (always within 24 h after sampling).

The chlorofluorocarbons CFC-12, CFC-11, CFC-113 and the halogenated tracers CH_3CCl_3 and CCl_4 were measured on a purge and trap GC/ECD system. A volume of 31 mL water was injected on to the purge and trap unit, where the samples were purged for 5 min with nitrogen at a flow rate of 80 mL/min. The components were trapped in an open bore 1/16″ trap cooled to low temperatures in the headspace immediately over liquid nitrogen. The analytes were thermally desorbed at 100 °C and injected onto a DB624 column (75 m × 0.53 mm). The precision for CFC-12 is estimated at 2%, and the limit of detection at 0.02 pmol/kg.

Determinations of SF_6 were made with a purge and trap coupled to gas chromatography with electron capture detection (GC/ECD). A volume 356 mL of seawater was injected into an evacuated strip tower and subsequently purged with nitrogen for 5 min at 100 mL/min. The SF_6 was trapped in a 1/16″ ID cold trap filled with Carboxen-1000 and trap kept at −60 °C. The sample was thermally desorbed and injected onto a MS 5 A column (3 m × 1/8″) and then refocused on a 1/32″ Carboxen-1000 packed trap kept at −130 °C, from which it was thermally desorbed onto a Porabond Q PLOT column (0.32 mm ID × 30 m) kept isothermally at 100 °C. The analytical precision of the method was estimated at 2% and the detection limit is estimated to 0.1 fmol kg^{-1}. The samples were calibrated vs. calibrated air obtained from CMDL/NOAA, Boulder Colorado, and are reported on the GMD2000 scale.

For this work, we have used CFC-12 data to calculate the mean age for samples with a CFC-12 concentration less than 450 ppt, and SF_6 data (if available) for more recently ventilated waters (i.e. [CFC-12] > 450 ppt). The reason for this is the slow atmospheric growth rate for CFC-12 since the mid-1990s, whereas SF_6 has increased almost linearly since about 1990. For older samples (i.e. [CFC-12] < 450 ppt), the higher concentration of CFC-12 compared to SF_6 favours the use of CFC-12 for the age calculations (Tanhua et al., 2008). We calculated the tracer age by fitting the measured concentration to the atmospheric history of the tracers. We adopted the time-dependent saturation of CFCs (Tanhua et al., 2008), i.e. assuming that the saturation was 86% up to 1989 after

which it increased linearly to 100% by year 1999, whereas the saturation of SF_6 is set at 85%. The assumption of an uncertainty of the saturation of 5% transforms to an uncertainty in the tracer age of ± 1 year for water with tracer age <50 years. The mean age was calculated using the TTD method (Waugh et al., 2003) with the assumption that the transit time distribution (TTD) can be represented by an inverse Gaussian distribution, where the mixing is represented by the mean age, Γ, and the width of the TTD, Δ. We further assume that these two parameters are of the same magnitude in the Arctic Ocean, see Tanhua et al. (2009).

3. Result and discussion

3.1. Dissolved inorganic carbon

The nutrient maximum in the water column is associated with an oxygen minimum and a maximum in the partial pressure of carbon dioxide, or here expressed as fugacity (fCO_2), and DIC (Fig. 2). It has long been known that the source of this nutrient maximum is the Chukchi Sea region and it has been suggested that the nutrient rich water leaves the shelf mainly in three regions: Barrow Canyon, Central Channel and Herald Valley (e.g. Weingartner et al., 2005). It is however unknown if there is a large variability in the magnitude of these outflows, both annually and inter-annually. Signatures of the nutrient maximum hanging on the continental margin off the Barrow Canyon and Hanna Shoal, east of the Central Channel, have been observed within the extensive studies of the SBI project (e.g. Codispoti et al., 2005, 2009). Our data support an outflow in the Herald Valley, an outflow that can be traced by the elevated phosphate concentrations and deficit in oxygen along the bottom from the latitude 71.4°N to the mouth north of 72.5°N (Fig. 3).

The high nutrient water also has very high fCO_2 values, up to more than 1000 µatm, well illustrating the continental shelf pump effect. The phosphate concentrations increase and the

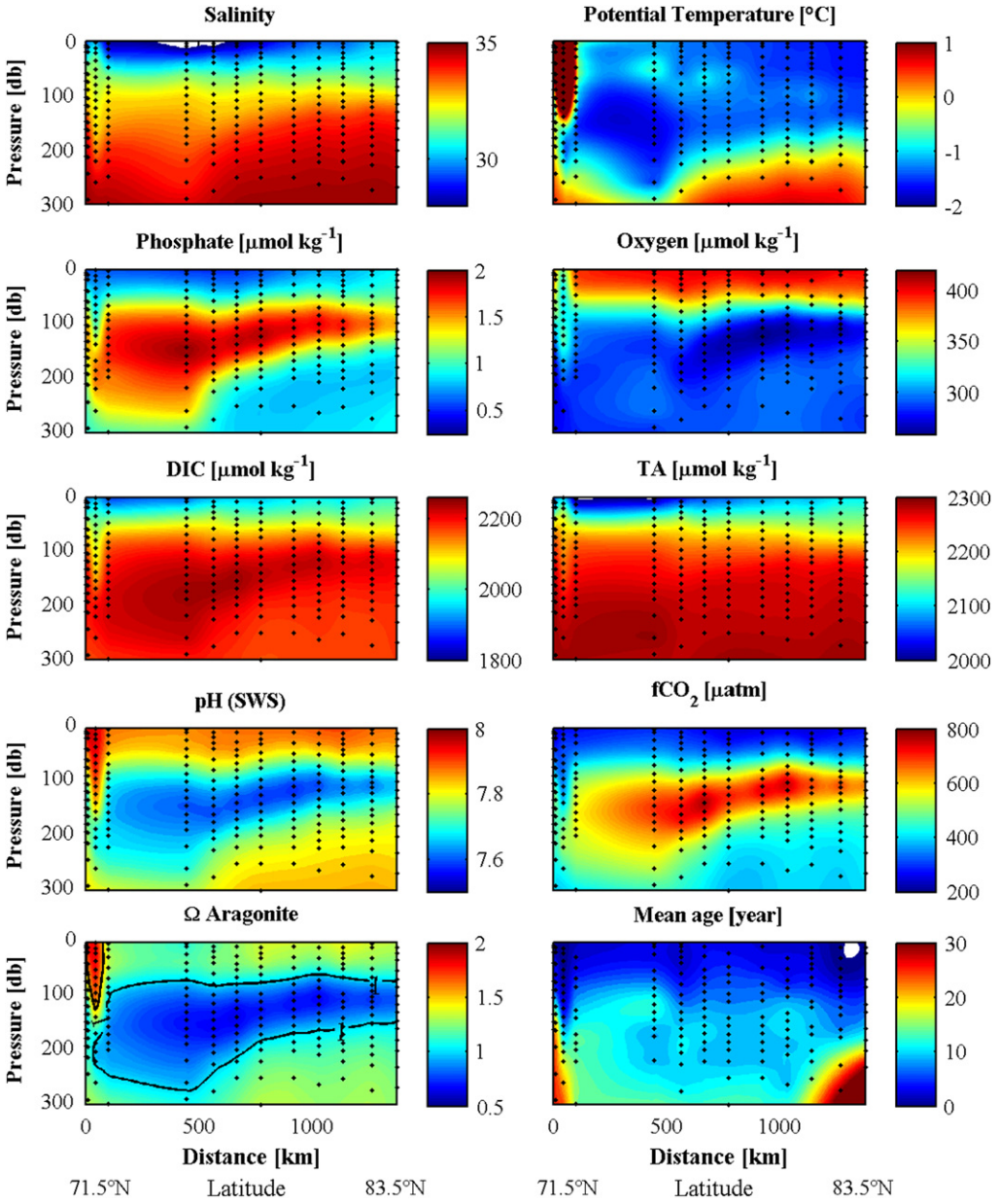

Fig. 2. Property distributions in the top 300 m along the Beringia stations of Fig. 1. The pH values are given on the seawater scale at a temperature of 15 °C and at 1 atm pressure, while the fCO_2 and $\Omega_{aragonite}$ are given at insitu temperature and pressure.

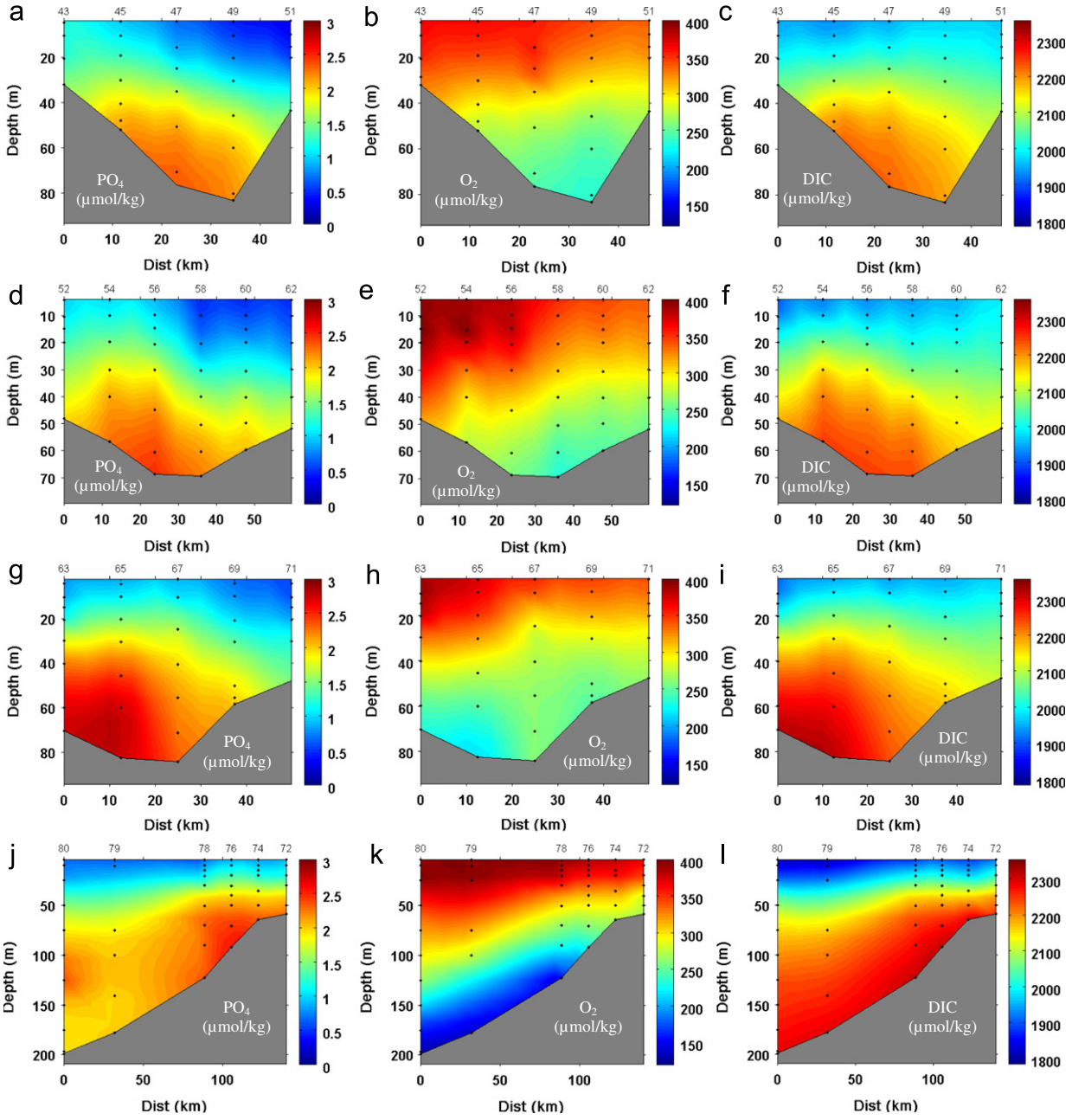

Fig. 3. Sections in the Herald Valley of phosphate, oxygen and dissolved inorganic carbon (DIC). The locations of the sections are shown in Fig. 1, and are located at approximate latitudes of 71.4°N (a, b and c), 71.9° (d, e and f), 72.3°N (g, h and i) and 72.8 to 74.0°N (j, k and l). Sections a to i have west to the left and east to the right, while sections j, k and l have north to the left and south to the right.

oxygen concentration decreases from the south towards the north, which can either be a result of variability in the source areas or a sign of how far the winter signature of high salinity bottom water has reached at the time of the study.

It is not only the Chukchi Sea that contributes waters to the nutrient maximum of the Canadian Basin. We show that waters with similar properties are found at the continental slope north of the eastern East Siberian Sea (Fig. 4), strongly indicating that nutrient rich water is exported also from this shelf. The nutrient maximum as seen by the high phosphate concentration extends at least to the deepest station visited (about 1100 m bottom depth), with the highest concentration at a depth of ~100 m and closest to the shelf (Fig. 4b). A maximum in fCO_2 follows the phosphate maximum with the magnitude decreasing to the north (Fig. 4a). There also is a maximum in the DIC signal but it is not as apparent as the background level is much higher relative to the increase at the nutrient maximum (Fig. 4d). Furthermore, the DIC concentration has a strong relationship with salinity and the nutrient maximum is located in the halocline which further masks the DIC maximum. The impact on TA from decaying organic matter, which should give a decrease that is equal to the increase in nitrate is also masked by the salinity relationship (Fig. 4c). The pH^{ssw} (at 15 °C) is very low at the shelf break, increasing to the north (Fig. 4e) also reflected in the $\Omega_{aragonite}$ has a large minimum with values below 1 (Fig. 4f), i.e. undersaturation with respect to aragonite. The decrease in the nutrient maximum signature from the shelf slope into the deep basin indicates the source being the shelf and supports the conclusion of the East Siberian Sea being one source region for this water. Likely the nutrient maximum water flows to the east after leaving

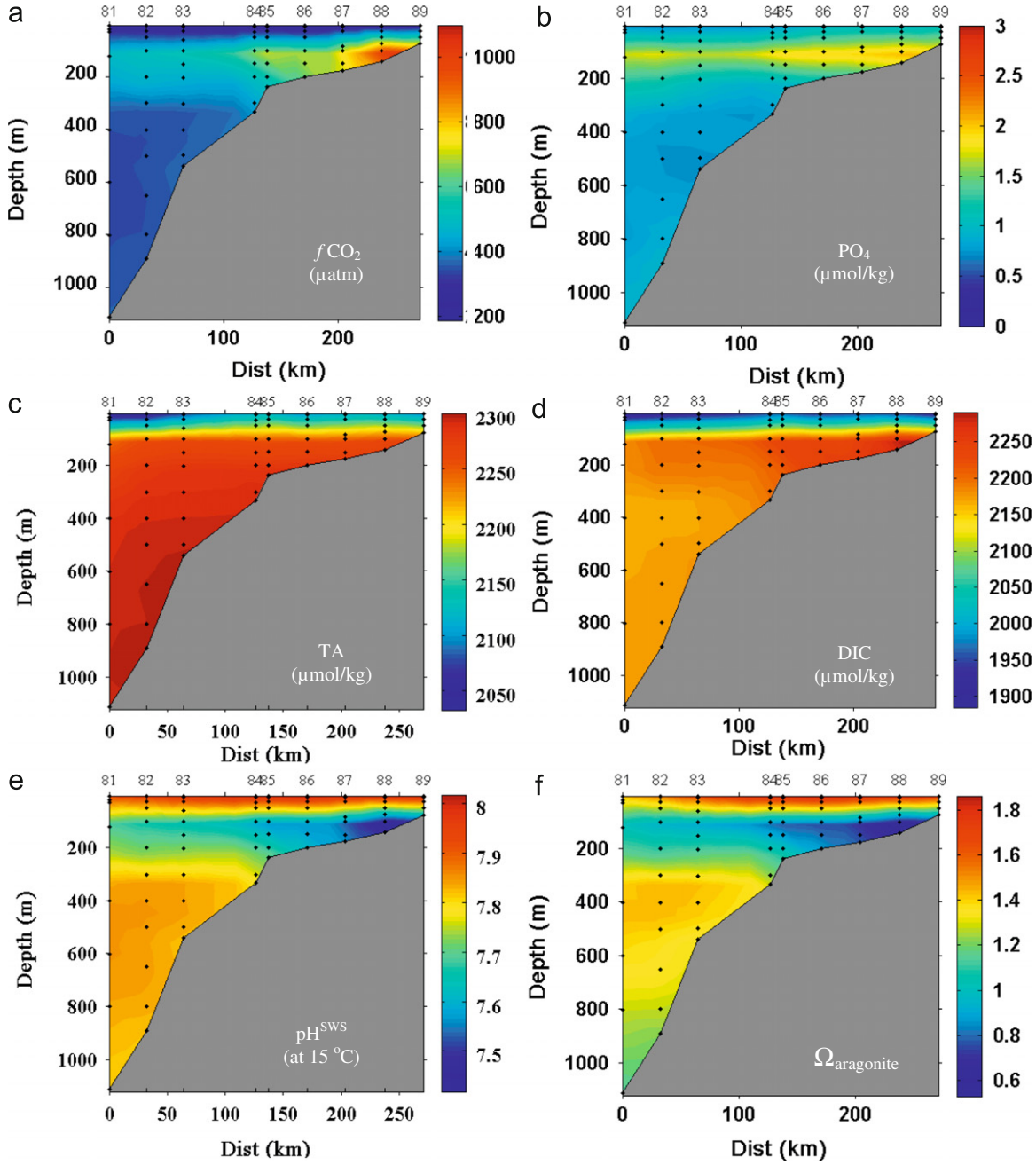

Fig. 4. fCO_2 (a), phosphate (b), total alkalinity (c) total dissolved inorganic carbon (d), pH^{sws} at 15 °C (e), and degree of aragonite saturation (f) along the section across the continental slope of the Northern East Siberian Sea.

the East Siberian Sea, across and around the Chukchi Cap. In our 2005 study, it had detached from the continental slope east of the Barrow Canyon as the strongest signal was observed off the slope (Fig. 2).

Our section into the Canada Basin (Fig. 2) illustrates that the UHL properties are confined to the Beaufort Gyre and have a mean age within the nutrient maximum layer of 12 ± 5 years for phosphate values > 1.5 µmol/kg. The age is lower along the continental margin which supports a boundary current of relatively recently ventilated water. It is possible that the origin of this water can vary with time. This feature shows that the typical properties of the UHL cannot be assigned a specific depth layer as it varies within the Canada and Makarov Basins, especially along its margins.

The DIC maximum associated with the nutrient maximum (UHL) along the section of Fig. 2 is less apparent than the phosphate maximum due to the large DIC background. However, in a plot of DIC versus salinity the maximum is clearly seen (Fig. 5a). It is also seen that this maximum is spread over a broad salinity range centered at a salinity just over 33. This is a somewhat lower salinity than that of the maximum during the SBI study in 2002 (Bates et al., 2005) and in 2004 (Mathis et al., 2009), but in those studies it was still associated with the nutrient maximum. Hence, it seems that the salinity of the nutrient maximum is variable during these studies, even if the maximum in DIC is stretched out over a wide salinity range. Nevertheless, it is possible that the salinity variability is due to changes in brine production from sea ice formation.

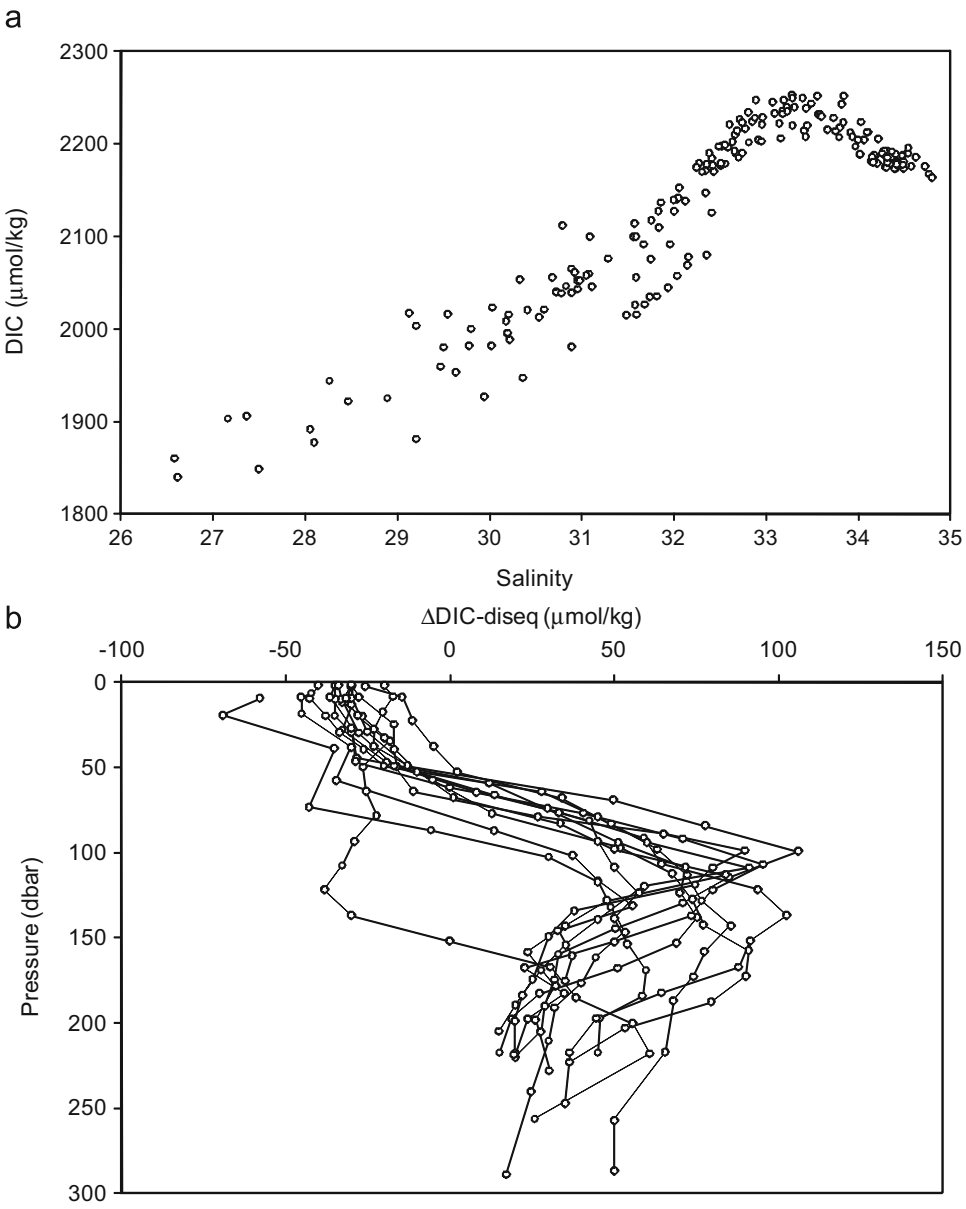

Fig. 5. Dissolved inorganic carbon (DIC) versus salinity (a), and profiles of DIC deviation from saturation (ΔDIC^{diseq}) at the time the water was in contact with the atmosphere (b). See text for a further explanation.

The surface water has low salinities ($S < 30$) as a result of large supply of river water as well as addition of sea ice melt water during the summer season (Cooper et al., 2005; Jones et al., 2008). In these waters the DIC concentration is impacted mainly by biological primary production, specifically in the shelf seas, while in the waters of the nutrient maximum it is mainly impacted by decay of organic matter. In principle, this impact could be quantified from the change in nutrients, but as there are several source waters and local processes that effect the source concentrations of the nutrients, such a computation has large uncertainties. Instead we make a quantitative estimate based on the deviation of DIC from equilibrium with the atmosphere.

3.1.1. DIC-deviation from equilibrium

The deviation of DIC from a water sample in equilibrium with the atmosphere (DIC^{diseq}) is computed as the difference between the measured DIC concentration and the calculated equilibrium DIC concentration (DIC^{eq}_{TTD}) according to equation (1). The theoretical equilibrium DIC concentration as a function of time for each sample is computed using the matlab version of the software CO2SYS (Lewis and Wallace, 1998; van Heuven et al., 2009) and the constants of Merbach et al. (1973) refit by Dickson and Millero (1987). The measured temperature, salinity, alkalinity, silicate and phosphate values are used together with the annual average fCO_2 from the Barrow, Alaska/ice core records. We recognize that each water sample is a mixture of waters with different ages as represented by their transit time distribution (TTD), all with its own equilibrium concentration. In order to correct for mixing of the water, we use the TTD calculated from the tracer measurements, and the DIC^{eq}_{TTD} concentration is calculated as the integral of the TTD multiplied with their respective $DIC^{atm\text{-}eq}$ concentrations, similar to the method used by Freing et al. (2009):

$$\Delta DIC^{diseq} = DIC^{measured} - DIC^{eq}_{TTD} \quad (1)$$

This computation of the ΔDIC^{diseq} thus explicitly corrects for mixing in the water column of waters having been in contact with

the atmosphere at varying years having different atmospheric CO_2 partial pressures. As we assume that the TTD has an inverse Gaussian shape, the oldest contribution is ventilated before the instrumental pCO_2 record of Barrow, and thus our choice of using ice core records. Furthermore, it is not obvious at what month the water investigated left contact with the surface as sea ice formation start already in September, and for this reason we use the annual mean pCO_2.

The computed ΔDIC^{diseq} values show negative values (undersaturation) in the surface water (down to ~50 m) for all the Beringia stations in the Canada Basin and then turn positive (oversaturation) with a maximum at depths between 100 and 200 m depth (Fig. 5b). One station deviates from this pattern and has negative values down to 150 m. This station is located just off the shelf break at 2090 m bottom depth, and the salinity, nutrient and oxygen signatures are all similar to those in the top ~50 m of the other stations, suggesting an intrusion to this depth of well ventilated surface water.

In order to quantify the carbon excess in the upper water masses we divide each profile (Fig. 5b) into two layers: one from the surface down to the level where ΔDIC^{diseq} shifts from negative to positive, and a second within the nutrient maximum layer, here defined from where ΔDIC^{diseq} turns positive down to the depth where the phosphate concentration decreases below 1 μmol kg^{-1} (Fig. 2 and Table 1). Both these two layers are predominately of Chukchi–East Siberian Shelves origin (Bates and Mathis, 2009). The integrated excess carbon as computed from the ΔDIC^{diseq} for each layer of every station profile is presented in Table 1.

The surface water over the Chukchi Sea area has a low pCO_2 values (e.g. Bates and Mathis, 2009; Fransson et al., 2009) and this water is exported to the deep central basin before being equilibrated with the atmosphere. The resulting ΔDIC^{diseq} excess in the surface layer is typical in the range −0.9 to −1.6 mol m^{-2} with a few exceptions. Close to the continental margin, at stations 2–4, the excess is very low, which likely is a result of interaction between the shelf outflow and a boundary current. The former supplies water that has recently experienced primary production and the latter brings water from the west with a weaker signal of remineralization of organic matter. These effects are also reflected in the depths of the surface layer as well as in the salinity at the interface between the two layers (Table 1). The excess in the nutrient maximum layer shows an increasing trend from the shelf slope towards station 8 after which it slowly decreases towards the north. The low excess at the shelf slope is a result of the deep upper boundary of this layer and somewhat lower ΔDIC^{diseq} value compared to that over the deep basin. The maximum excess at station 8 reflects the deep lower boundary that continuously shallows when moving to the north, resulting in a thickness of the nutrient maximum layer at station 8 of 234 m decreasing to 75 m at station 20. This depth distribution of the nutrient maximum layer is also clearly seen in Fig. 2.

Table 1
The excess dissolved inorganic carbon for the surface water and nutrient maximum layer (NML) relative to the computed ΔDIC^{diseq}. Noted are also the corresponding depths of these layers and the salinity at the boundary between them.

Stn. #	Latitude (N°)	C^{excess} (mol m^{-2})		Depth (m)		Salinity
		Surface	NML	Surface	NML	At boundary
2	71.5	−2.1	4.0	73	209[a]	32.23
3	71.6	−3.5	5.7	87	240	32.41
4	71.9	−3.9	4.1	152	256	32.15
5	72.4	−1.3	7.9	47	217	30.89
8	75.5	−0.4	14.4	53	287	31.68
9	76.6	−0.9	10.1	57	223	31.09
11	77.5	−0.9	9.0	50	182	30.67
12	78.5	−1.4	7.0	45	183	30.73
14	79.5	−1.4	6.5	62	167	30.73
15	80.4	−1.0	7.4	49	160	30.93
17	81.4	−1.6	5.4	49	154	30.95
19	82.5	−1.4	4.1	64	134	31.08
20	83.5	−1.0	3.8	68	143	31.29

[a] The bottom depth of this station.

The mean carbon excess over the deep basin (stations 8–20) is -1.1 ± 0.4 and 7.5 ± 3.3 mole m^{-2} or -14 ± 4 and 90 ± 40 g C m^{-2}, for the surface and nutrient maximum layer, respectively. The uncertainty in the estimates calculated as the variability, 1 sigma, between the stations. If the Arctic Ocean will become ice free in the future, the surface layer will be more exposed to atmospheric gas exchange, potentially reducing the undersaturation of CO_2 in the surface layer. If the surface layer becomes saturated with CO_2, this could add to a one time uptake of atmospheric CO_2 of a corresponding magnitude.

The carbon excess relative to the equilibrium with the atmosphere at the TTD age distribution within the nutrient maximum layer, 7.5 ± 3.3 mole m^{-2} or 90 ± 40 g C m^{-2}, can be considered as a result of the continental shelf carbon pump. It is not straightforward to quantify this on an annual basis as the age of the water along the investigated section is 12 ± 5 years and during this time horizontal mixing likely occurs. Hence, we take two approaches to get a quantitative estimate; one just comparing the areal excess with estimates of the export production within the Chukchi Sea, and the second to compute the excess over the whole of the Canadian Basin (considering the residence time) and compare this with estimates of total productivity within the Chukchi Sea.

The source of this excess carbon can be anywhere in the shelves that supply this water. The T/S property implies a winter water that either is formed on the shelf by brine rejection from sea ice production, or by cold saline water coming directly through the Bering Strait. Regardless, this water flows along the bottom and hence takes up decay products from the sediment surface to which organic matter has been supplied by the export productions in the Chukchi Sea. Production estimates vary from an average of 0.78 g C m^{-2} d^{-1} on the northeastern Chukchi Sea (Hill and Cota, 2005) based on ^{14}C measurements to net community production rates of 0.9($\pm$0.6) g C m^{-2} d^{-1} (Mathis et al., 2009). The latter is the mean of the shelf data from Table 4 in their article. Assuming a yearly production length of 120 days, there is a potential of an export to the sediment surface in the order of 100 g C m^{-2}. Kaltin and Anderson (2005) estimated the export production to 68 ± 8 g C m^{-2} by computing the consumption of phosphate in the water column during its flow over the Bering and Chukchi Seas. If this amount of organic matter is mineralized at the sediment surface and the decay products are added to the bottom water before it flows of into the deep central Arctic Ocean a corresponding excess will be found integrated over the depth of the nutrient maximum. However, to compare this export production (70 to 100 g C m^{-2}) with our observed excess over the deep Canadian Basin (90 ± 40 g C m^{-2}) it implies an annual supply to the nutrient maximum water from the shelf having the observed concentrations, which means that no horizontal mixing will impact the estimate. This is likely not the situation, but the relatively constant excess over the deep basin (Table 1) implies that the horizontal mixing will smooth the signal making the comparison relevant within the variability.

If the carbon excess, 7.5 ± 3.3 mol m^{-2} or 90 ± 40 g C m^{-2}, is representative of the whole of the $3.5 \cdot 10^{12}$ m^2 of the Canadian Basin (Makarov and Canada basins) the corresponding excess is $26 \pm 12 \cdot 10^{12}$ mol or $320 \pm 140 \times 10^{12}$ g C. Using the computed TTD age of the nutrient maximum of 12 ± 5 years results in the need for an annual supply of $2.2 \pm 1.5 \times 10^{12}$ mol or

$26 \pm 18 \times 10^{12}$ g C in order to maintain steady state condition (where the uncertainty include both the variability in excess and the uncertainty of the age). This number should hence quantify the total continental shelf pump from the Chukchi and East Siberian Seas, assuming that the tracers used to compute the TTD age and the CO_2 equilibrated at the same time.

If no buildup of organic matter occurs in the shelf sediment, i.e. steady state, the carbon excess found in the nutrient maximum of the central Arctic Ocean should equal the export production mainly in the Chukchi and East Siberian Seas. To our knowledge no such estimate has been done for the East Siberian Sea and they are few for the Chukchi Sea as well. Kaltin and Anderson (2005) took their computed phosphate consumption in the Bering and Chukchi Seas, converted it to carbon units and were multiplied by the volume flow through Bering Strait, to achieve a value of 17×10^{12} g C yr^{-1}. They do not report any uncertainty in this value, but considering the uncertainty of the data going into the computation it should be roughly 25%. One could also compare to the air to sea flux computations of Bates (2006), which based on seawater pCO_2 observations from the Chukchi Sea equals $29^{\circ} \pm 8 \times 10^{12}$ g C yr^{-1}. If this flux computation is a result of an annual net primary production, a corresponding carbon flux to the interior Arctic Ocean has to occur. All these three estimates are equal within their uncertainties.

However, these comparisons should not be taken as exact quantitative estimates, but are only done to put some credit to the magnitude of our estimate of the continental shelf pump of the Arctic Ocean Pacific shelves.

3.2. Calcium carbonate saturation

The calcium carbonate saturation state is heavily impacted by biological activity on a seasonal as well as spatial scale. Within the Arctic Ocean changes in salinity by the large input of rivers and by sea ice melt have large effects (Bates et al., 2009; Chierici and Fransson, 2009; Yamamoto-Kawai et al., 2009), mainly by lowering the concentration of calcium ions. The release of CO_2 from decaying organic matter decreases pH and results in a low degree of calcium carbonate saturation to a level that could cause aragonite and even calcite shells to dissolve, i.e. saturation state for aragonite, $\Omega_{aragonite} < 1$, and for calcite, $\Omega_{calcite} < 1$. This is evident in the nutrient maximum layer of the Canadian Basin (Fig. 2) and in the waters that feed this layer from the shelf (Fig. 4). These very low $\Omega_{aragonite}$ values are caused by decay of organic matter and are not yet that much impacted by anthropogenic CO_2, and thus it is likely that large parts of the bottoms of the East Siberian and Chukchi Seas have been exposed to under-saturated aragonite conditions for many years. However, since the upper layers of the Arctic Ocean are generally only slightly over-saturated with respect to aragonite, the Arctic Ocean is therefore particularly sensitive to increasing DIC concentrations, e.g. decreasing pH (Jutterström and Anderson, 2005) due to changes in biology or due to input of anthropogenic carbon.

In order to estimate the anthropogenic effects on the central Arctic Ocean pH and $CaCO_3$ saturation, we use the estimates of anthropogenic carbon concentrations (C_{ant}) derived from SF_6 and CFC-12 data using the TTD method (Tanhua et al., 2009). The measured DIC and total alkalinity data from the Beringia cruise in 2005 (time-invariable total alkalinity is assumed) is then used to calculate contemporary pH as well as pre-industrial pH by subtracting the C_{ant} signal from the measured DIC. Additionally, we make a projection of the future pH and $CaCO_3$ saturation by assuming continuous exponential increase of anthropogenic carbon in the atmosphere, and constant Arctic Ocean circulation. Since we know the TTD of the water column, the concentration of any other tracer can be calculated for any time if the input function is known, and the anthropogenic carbon is treated like a tracer in this approach.

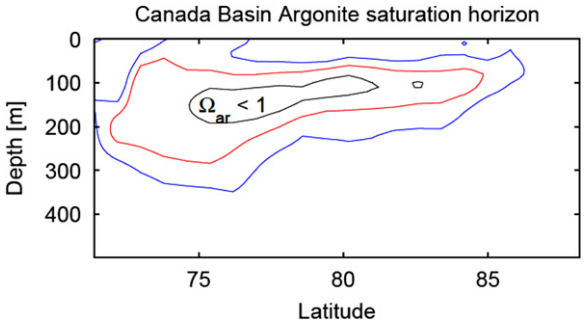

Fig. 6. Section of the aragonite saturation in the Canada Basin during the Beringia 2005 cruise (south to the left and north to the right) showing the contour equal to 1 (i.e. $\Omega_{ar}=1$): black line for pre-industrial; red line for the contemporary; and blue line for predicted extension in year 2050. (For interpretation of the references to colour in this figure legend, the reader is referred to the web version of this article.)

The difference between the pre-industrial pH and contemporary pH (ΔpH) is in excess of 0.1 pH units in the surface waters. The contemporary $\Omega_{aragonite}$ has a minimum of 0.6 at a depth around 150 m, with the shallowest depth with under-saturation being ~70 m (Fig. 6). Even calcite (not shown) is under-saturated at a few stations at the depth where $\Omega_{aragonite}$ has its minima. Fig. 6 show clearly that the zone of aragonite under-saturation has grown significantly since pre-industrial times, and is likely to continue to expand in the future. The recent decrease in salinity of the surface waters in some regions of the Canada Basin as a result of increased sea ice melt has resulted in under-saturation of aragonite (e.g. Yamamoto-Kawai et al., 2009). However, even without this freshening the aragonite under-saturation could reach the surface by year 2050. The acidification of the Arctic Ocean waters due to the input of anthropogenic carbon has further led to an upward shift of the average aragonite saturation horizon by about 190 m (from 2080 to 1890 m, on average). Since the system is already close to being under-saturated for the entire water column, we predict that by 2050 the aragonite saturation horizon will have propagated upward to about 1000 m depth, nearly closing the gap between the sub-surface and deep water zones of aragonite under-saturation. It appears likely that within a century we will see an Arctic Ocean that is entirely under-saturated in respect to aragonite.

The anthropogenic input of CO_2 to the Arctic Ocean has only marginally shifted the calcite saturation horizon since pre-industrial times (this horizon is situated below depths where the C_{ant} has as penetrated in large amounts). However, in 2050 even calcite is likely to be under-saturated between 100 and 200 m depth in most places in the Canada Basin. This might have potentially harmful effects on aragonite and calcite-shell building organisms, such as Rhodolithen (e.g. *Lithothomnion arctica*), coral-like algae dominating the benthic in, for instance, Svalbard if this water reaches the shelf areas.

4. Summary and conclusion

Previous work has discussed the importance of the continental shelf pump. We have shown that in the Arctic Ocean the DIC signal of the upper waters in the Canadian Basin is mainly impacted by biological processes (not considering mixing) and that the continental shelf pump of CO_2 from the Pacific sector of the Arctic Ocean results in an excess of carbon in sub-surface

waters of the Canadian Basin. We have showed that not only the Chukchi Sea but also the East Siberian Sea is an important source area for this continental shelf pump. The resulting excess carbon is distributed at depths between ~50 and 250 m to a magnitude that equals $320 \pm 140 \times 10^{12}$ g C when integrated over the whole area of the Canadian Basin. Taking into consideration the TTD age of these waters, the annual continental shelf pump is $26 \pm 18 \times 10^{12}$ g C of carbon into the Canadian Basin of the Arctic Ocean. A result of this active continental shelf pump is that the surface water of the central Arctic Ocean gets under-saturated with respect to CO_2, an under-saturation that persist as the sea ice coverage of the region hampers air–sea exchange. The magnitude at present equals -14 ± 4 g C m^{-2} but with decreasing sea ice coverage, or even disappearance in summer time, an increased air–sea flux of CO_2 will likely decrease this deficit.

From direct measurements we find that the nutrient maximum water as well as its sources on the shelves is extensively impacted by organic matter decay products, and that the pH has decreased to levels where some forms of biogenic calcium carbonate might dissolve. Aragonite is extensively under-saturated and calcite is slightly under saturation at some stations. This has clear implications for future climate change. The under-saturation had not yet reached the surface in the presented 2005 study, but applying estimates of anthropogenic carbon concentrations using the TTD method we show how the extent of the area under-saturated with respect to aragonite has increased within the nutrient maximum of the Canadian Basin from pre-industrial times to date, and will reach the surface by year 2050. The aragonite under-saturation will be amplified when the pCO_2 increases in the PML as a result of uptake from the atmosphere as the summer sea ice coverage decreases. However, it has been shown that the freshening of the surface waters due to increasing sea ice melt in the Canada Basin already has resulted in under-saturation (e.g. Yamamoto-Kawai et al., 2009). The combination of both lowering of salinity and the saturation state of calcium carbonate will result in a multistress to the biota. Our result shows that even without any dramatic change in surface water salinity the surface water will be under-saturated with respect to aragonite in the near future as a result of the expansion of the halocline layer respiratory CO_2 max by anthropogenic CO_2 uptake.

Acknowledgments

This study was performed under the logistic support of the Swedish Polar Research Secretariat and was been supported by Grants by the Swedish Research Council and the European Union projects, CarboOcean (Contract no. 511176-2), DAMOCLES (Contract no. 018509-2) and EPOCA (Contract no. 211384) and the Canada Panel on Energy Research and Development (EPJ). Publication no. 11 from Tellus—The Centre of Earth Systems Science at University of Gothenburg.

References

Anderson, L.G., Turner, D.R., Wedborg, M., Dyrssen, D., 1999. Determination of total alkalinity and total dissolved inorganic carbon. In: Kremling, K., Ehrhardt, M. (Eds.), Methods of Seawater Analysis third ed. VCH, Weinheim, Germany, pp. 127–148.

Anderson, L.G., Kaltin, S., 2001. Carbon fluxes in the Arctic Ocean—potential impact by climate change. Polar Res. 20 (2), 225–232.

Anderson, L.G., Olsen, A., 2002. Air–sea flux of anthropogenic carbon dioxide in the North Atlantic. Geophys. Res. Lett. 29 (17, doi:10.1029/2002GL014820.

Bates, N.R., 2006. Air–sea CO_2 fluxes and the continental shelf pump of carbon in the Chukchi Sea adjacent to the Arctic Ocean. J. Geophys. Res. 111, C10013, doi:10.1029/2005JC003083.

Bates, N.R., Hansell, D.A., Moran, S.B., Codispoti, L.A., 2005. Seasonal and spatial distributions of particulate organic matter (POM) in the Chukchi Sea. Deep-Sea Res. Part II 52, 3324–3343.

Bates, N.R., Mathis, J.T., Cooper, L.W., 2009. The effect of ocean acidification on biologically induced seasonality of carbonate mineral saturation states in the Western Arctic Ocean. J. Geophys. Res. 114, C11007, doi:10.1029/2008JC004862.

Bates, N.R., Mathis, J.T., 2009. The Arctic Ocean marine carbon cycle: evaluation of air–sea CO_2 exchanges, ocean acidification impacts and potential feedbacks. Biogeosciences 6, 2433–2459.

Borges, A.V., Frankignoulle, M., 1999. Daily and seasonal variations of the partial pressure of CO_2 in surface seawater along Belgian and southern Dutch coastal areas. J. Mar. Sys. 19 (4), 251–266.

Borges, A.V., Frankignoulle, M., 2002. Distribution and air–water exchange of carbon dioxide in the Scheldt plume off the Belgian coast. Biogeochemistry 59, 41–47.

Borges, A.V., Delille, B., Frankignoulle, M., 2005. Budgeting sinks and sources of CO_2 in the coastal ocean: diversity of ecosystems counts. Geophys. Res. Lett., 32.

Bozec, Y., Thomas, H., Elkalay, K., de Baar, H.J.W., 2005. The continental shelf pump for CO_2 in the North Sea—evidence from summer observation. Mar. Chem. 93, 131–147.

Carmack, E., Wassmann, P., 2006. Food webs and physical–biological coupling on pan-Arctic shelves: unifying concepts and comprehensive perspectives. Prog. Oceanogr. 71, 446–477.

Chen, C.-T.A., Borges, A.V., 2009. Reconciling opposing views on carbon cycling in the coastal ocean: continental shelves as sinks and near-shore ecosystems as sources of atmospheric CO_2. Deep-Sea Res. Part II 56, 578–590, doi:10.1016/j.dsr2.2009.01.001.

Chierici, M., Fransson, A., 2009. Calcium carbonate saturation in the surface waters of the Arctic Ocean: undersaturation in freshwater influenced shelves. Biogeosciences 6, 2421–2432.

Clayton, T.D., Byrne, R.H., 1993. Spectrophotometric seawater pH measurements: total hydrogen ion concentration scale calibration of m-cresol purple and at-sea results. Deep-Sea Res. Part I 40, 2115–2129.

Codispoti, L.A., Flagg, C., Kelly, V., Swift, J.H., 2005. Hydrographic conditions during the 2002 SBI process experiments. Deep-Sea Res. Part II 52, 3199–3226.

Codispoti, L.A., Flagg, C., Swift, J., 2009. Hydrographic conditions during the 2004 SBI process experiments. Deep-Sea Res. Part II 56, 1144–1163.

Cooper, L.W., Benner, R., McClelland, J.R., Peterson, B.J., Holmes, R.M., Raymond, P.A., Hansell, D.A., Grebmeier, J.M., Codispoti, L.A., 2005. The linkage between runoff, dissolved organic carbon, and the stable oxygen isotope composition of seawater and other water mass indicators in the Arctic Ocean. J. Geophys. Res. 110, G02013, doi:10.1029/2005JG000031.

De Haas, H., Van Weering, T.C.E., De Stigter, H., 2002. Organic carbon in shelf seas: sinks or sources, processes and products. Cont. Shelf Res. 22, 691–717.

Dickson, A.G., Millero, F.J., 1987. A comparison of the equilibrium constants for the dissociation of carbonic acid in seawater media. Deep-Sea Res. 34, 1733–1743.

Ducklow, H.W., McAllister, S.L., 2005. Biogeochemistry of carbon dioxide in the coastal oceans, in the Sea. In: Robinson, A.R., Brink, K.H. (Eds.), The Global Coastal Ocean: Multiscale Interdisciplinary Processes, 13. John Wiley, Hoboken, NJ.

Frankignoulle, M., Borges, A.V., 2001. European continental shelf as a significant sink for atmospheric carbon dioxide. Global Biogeochem. Cycles 15 (3), 569–576.

Fransson, A., Chierici, M., Nojiri, Y., 2009. New insights into the spatial variability of the surface water carbon dioxide in the varying sea ice condition in the Arctic Ocean. Cont. Shelf Res. 29, 1317–1328.

Freing, A., Wallace, D.W.R., Tanhua, T., Walter, S., Bange, H., 2009. North Atlantic production of nitrous oxide in the context of changing atmospheric levels. Global Biogeochem. Cycles 23, GB4015, doi:10.1029/2009GB003472.

Gordon, L.I., Jennings, J.C., Ross, A.A., Krest, J.M., 1993. A suggested protocol for continuous flow automated analysis of seawater nutrients (phosphate, nitrate, nitrite and silicic acid) in the WOCE Hydrographic Program and the Joint Global Ocean Fluxes Study, WOCE Hydrographic Program Office, Methods Manual WHPO91–1, (〈http://whpo.ucsd.edu/manuals/pdf/91_1/ gordnut.pdf〉).

Grebmeier, J.M., Harvey, H.R., 2005. The Western Arctic shelf–basin interaction (SBI) project: an overview. Deep-Sea Res. Part II, 3109–3115.

Haraldsson, C., Anderson, L.G., Hassellöv, M., Hulth, S., Olsson, K., 1997. Rapid, high-precision potentiometric titration of alkalinity in the ocean and sediment pore waters. Deep-Sea Res. Part I 44, 2031–2044.

Hill, V.J., Cota, G.F., 2005. Spatial patterns of primary production in the Chukchi Sea in the spring and summer of 2002. Deep-Sea Res. Part II 52, 3344–3354.

Johnson, K.M., Sieburth, J.M., Williams, P.J., Brändström, L., 1987. Coulometric total carbon dioxide analysis for marine studies: automation and calibration. Mar. Chem. 21, 117–133.

Jones, E.P., Anderson, L.G., 1986. On the origin of the chemical properties of the Arctic Ocean halocline. J. Geophys. Res. 91, 10759–10767.

Jones, E.P., Anderson, L.G., Swift, J.H., 1998. Distribution of Atlantic and Pacific waters in the upper Arctic Ocean: implications for circulation. Geophys. Res. Lett. 25 (6), 765–768.

Jones, E.P., Anderson, L.G., Jutterström, S., Mintrop, L., Swift, J.H., 2008. Pacific freshwater, river water and sea ice meltwater across Arctic Ocean basins: results from the 2005 Beringia expedition. J. Geophys. Res. 113, C08012, doi:10.1029/2007JC004124.

Jutterström, S., Anderson, L.G., 2005. The saturation of calcite and aragonite in the Arctic Ocean. Mar. Chem. 94, 101–110.

Kaltin, S., Anderson, L.G., 2005. Uptake of atmospheric carbon dioxide in Arctic shelf seas: evaluation of the relative importance of processes that influence

pCO_2 in water transported over the Bering – Chukchi Sea shelf. Mar. Chem. 94, 67–79.
Kempe, S., 1995. Coastal seas: a net source or sink of atmospheric carbon dioxide? LOICZ/R and S/95-1. LOICZ, Texel, The Netherlands vi+27 pp.
Kempe, S., Pegler, K., 1991. Sinks and sources of CO_2 in coastal seas: the North Sea. Tellus 43B, 224–235.
Kinney, P., Arhelger, M.E., Burrell, D., 1970. Chemical characteristics of water masses in the Amundsen Basin of the Arctic Ocean. J. Geophys. Res. 75, 4097–4104.
Lee, K., Millero, F.J., 1995. Thermodynamic studies of the carbonate system in seawater. Deep-Sea Res. Part I 42, 2035–2061.
Lewis, E., Wallace, D.W.R., 1998. Program developed for CO_2 system calculations. ORNL/CDIAC-105. Carbon Dioxide Information Analysis Center, Oak Ridge National Laboratory, Department of Energy, Oak Ridge, Tennessee, U.S.
Lepore, K., Moran, S.B., Grebmeier, J.M., Cooper, L.M., Lalande, C., Maslowski, W., Hill, V., Bates, N.R., Hansell, D.A., Mathis, J.T., Kelly, R.P., 2007. Seasonal and interannual changes in particulate organic carbon export and deposition in the Chukchi Sea. J. Geophys. Res. 112, C10024, doi:10.1029/2006JC003555.
Mackenzie, F.T., Lerman, A., Ver, L.M., 1998. Role of continental margin in the global carbon balance during the past three centuries. Geology 26 (5), 423–426.
Mathis, J.T., Pickart, R.S., Hansell, D.A., Kadko, D., Bates, N.R., 2007a. Eddy transport of organic carbon and nutrients from the Chukchi Shelf: impact on the upper halocline of the western Arctic Ocean. J. Geophys. Res. 112, C05011, doi:10.1029/2006JC003899.
Mathis, J.T., Hansell, D.A., Kadko, D., Bates, N.R., Cooper, L.W., 2007b. Determining net dissolved organic carbon production in the hydrographically complex western Arctic Ocean. Limnol. Oceanogr. 52 (5), 1789–1799.
Mathis, J.T., Bates, N.R., Hansell, D.A., Babilia, T., 2009. Net community production in the northeast Chukchi Sea. Deep-Sea Res. II 56, 1213–1222.
Meĭnikov, I.A., Pavlov, G.L., 1978. Characteristics of organic carbon distribution in the waters of the Arctic Basin. Oceanology 18, 163–167.
Mehrbach, C., Culberson, C.H., Hawley, J.E., Pytkowicz, R.M., 1973. Measurement of the apparent dissociation constants of carbonic acid in seawater at atmospheric pressure. Limnol. Oceanogr. 18, 897–907.
Moore, R.M., Lowings, M.G., Tan, F.C., 1983. Geochemical profiles in the central Arctic Ocean: their relation to freezing and shallow circulation. J. Geophys. Res. 88, 2667–2674.
Mucci, A., 1983. The solubility of calcite and aragonite in seawater at various salinities, temperatures and at one atmosphere pressure. Am. J. Sci. 283, 781–799.
Nikiforev, Ye.G., Belysheva, Y.V., Blinov, N.I., 1966. The structure of water masses in the eastern part of the Arctic Ocean. Oceanology 6, 59–64.
Proshutinsky, A.Y., Johnson, M.A., 1997. Two circulation regimes of the wind-driven Arctic Ocean. J. Geophys. Res. 102, 12493–12514.
Proshutinsky, A., Bourke, R.H., McLaughlin, F.A., 2002. The role of the Beaufort Gyre in Arctic climate variability: seasonal to decadal climate scales. Geophys. Res. Lett. 29, 2100, doi:10.1029/2002gl015847.
Rudels, B., Jones, E.P., Anderson, L.G., Kattner, G., 1994. On the intermediate depth waters of the Arctic Ocean. In: Johannessen, O.M., Muench, R.D., Overland, J.E. (Eds.), The Polar Oceans and Their Role in Shaping the Global Environment. American Geophysical Union, Washington, DC, pp. 33–46.
Rudels, B., Anderson, L.G., Jones, E.P., 1996. Formation and evolution of the surface mixed layer and halocline of the Arctic Ocean. J. Geophys. Res. 101, 8807–8821.
Rudels, B., Jones, E.P., Schauer, U., Eriksson, P., 2004. Atlantic sources of the Arctic Ocean surface and halocline waters. Polar Res. 23, 181–208.
Semiletov, I.P., Pipko, I.I., Repina, I., Shakhova, N.E., 2007. Carbonate chemistry dynamics and carbon dioxide fluxes across the atmosphere–ice–water interfaces in the Arctic Ocean: pacific sector of the Arctic. J. Mar. Sys. 66, 204–226.
Tanhua, T., Waugh, D.W., Wallace D.W.R., 2008. Use of SF_6 to estimate anthropogenic carbon in the upper ocean. J. Geophys. Res.—Oceans, 10.1029/2007JC004416.
Tanhua, T., Jones, E.P., Jeansson, E., Jutterström, S., Smethie Jr., W.M., Wallace, D.W.R., Anderson, L.G., 2009. Ventilation of the Arctic Ocean: mean ages and inventories of anthropogenic CO_2 and CFC-11. J. Geophys. Res. 114, C01002, doi:10.1029/2008JC004868.
Thomas, H., Bozec, Y., Elkalay, K., De Baar, H.J.W., 2004. Enhanced open ocean storage of CO_2 from shelf sea pumping. Science 304, 1005–1008.
Tsunogai, S., Watanabe, S., Sato, T., 1999. Is there a "continental shelf pump" for the absorption of atmospheric CO_2? Tellus 51B, 701–712.
van Heuven, S., Pierrot, D., Lewis, E., Wallace, D.W.R., 2009. MATLAB Program Developed for CO_2 System Calculations. ORNL/CDIAC-105b. Carbon Dioxide Information Analysis Center, Oak Ridge National Laboratory, Department of Energy, Oak Ridge, Tennessee, U.S.
Walsh, J.J., 1991. Importance of continental margins in the marine biogeochemical cycling of carbon and nitrogen. Nature 350, 53–55.
Wang, S.-L., Chen, C.-T.A., Hong, G.-H., Chung, C.-S., 2000. Carbon dioxide and related parameters in the East China Sea. Cont. Shelf Res. 20, 525–544.
Wang, J., Cota, G.F., Comiso, J.C., 2005. Phytoplankton in the Beaufort and Chukchi Seas: distribution, dynamics, and environmental forcing. Deep-Sea Res. Part II 52, 3355–3368.
Wassmann, P., Reigstad, M., Haug, T., Rudels., B., Carroll, M.L., Hop, H., Wing Gabrielsen, G., Falk-Petersen, S., Denisenko, S.G., Arashkevich, E., Slagstad, D., Pavlov, O., 2006. Food webs and carbon flux in the Barents Sea. Prog. Oceanogr. 71, 232–287.
Waugh, D.W., Hall, T.M., Haine, T.W.N., 2003. Relationship among tracer ages. J. Geophys. Res., 108, doi:10.1029/2002JC001325.
Weingartner, T.J., Aagaard, K., Woodgate, R.A., Danielson, S., Sasaki, Y., Cavalieri, D., 2005. Circulation on the north central Chukchi Sea shelf. Deep-Sea Res. Part II 52, 3150–3174.
Weiss, R.F., 1974. Carbon dioxide in water and seawater: the solubility of a non-ideal gas. Mar. Chem. 2, 203–215.
Yamamoto-Kawai, M., Mclaughlin, F.A., Carmack, E.C., Nishino, S., Shimada, K., 2009. Aragonite undersaturation in the Arctic Ocean: effects of ocean acidification and sea ice melt. Science 326, 1098–1100 1010.1126/science.1174190.